# The Search for Million Degree Gas through the $N_{VII}$ Hyperfine Line

Joel N. Bregman – University of Michigan

Jimmy A. Irwin – University of Michigan

The Astrophysical Journal, 666:139–146, 2007 September 1


# THE SEARCH FOR MILLION DEGREE GAS THROUGH THE N VII HYPERFINE LINE

Joel N. Bregman and Jimmy A. Irwin
Department of Astronomy, University of Michigan, Ann Arbor, MI 48109; jbregman@umich.edu, jairwin@umich.edu
*Received 2006 November 15; accepted 2007 May 12*

## ABSTRACT

Gas in the million degree range occurs in a variety of astronomical environments, and it may be the main component of the elusive missing baryons at low redshift. The N VII ion is found in this material and has a hyperfine spin-flip transition with a rest frequency of 53.042 GHz, which can be observed for $z > 0.1$, when it is shifted into a suitably transparent radio band. We used the 42–48 GHz spectrometer on the Green Bank Telescope to search for both emission and absorption from this N VII transmission. For absorption studies, 3C 273, 3C 279, 3C 345, and 4C +39.25 were observed, but no features were seen above the 5 $\sigma$ level. For emission line studies, we observed Abell 1835, Abell 2390, and the star-forming galaxy PKS 1345+12, but no features were seen exceeding 5 $\sigma$. We examine whether the strongest emission feature, in Abell 2390 (3.7 $\sigma$), and the strongest absorption feature, toward 4C +39.25 (3.8 $\sigma$), might be expected from theoretical models. The emission feature would require $\sim 10^{10}\ M_\odot$ of $10^6$ K gas, which is inconsistent with X-ray limits for the O VII K$\alpha$ line, so it is unlikely to be real. The N VII absorption feature requires a N VII column of $6 \times 10^{16}$ cm$^{-2}$, higher than model predictions by at least an order of magnitude, which makes it inconsistent with model expectations. The individual observations were less than 1 hr in length, so for lengthy observations, we show that N VII absorption line observations can begin to be useful in the search for hot intergalactic gas.

*Subject headings:* cooling flows — galaxies: clusters: individual (Abell 1835, Abell 2390) — galaxies: starburst — quasars: absorption lines — radio lines: general

*Online material:* color figures

## 1. INTRODUCTION

The study of hot gas at temperatures of $10^6$ K or greater has been the province of X-ray astronomy, since the resonance transitions of the most common ionic states occur in the 0.1–8 keV range. Hot gas is found to be very common in a wide range of astronomical objects, such as galaxy clusters, early-type galaxies, and starburst galaxies, where it is seen in emission. In addition, most of the baryons in the local universe are predicted to have temperatures of $10^5$–$10^7$ K, filling the volumes of modest overdensity cosmological filaments, sometimes referred to as the "cosmic web" (this is also the warm-hot intergalactic medium, or WHIM). This gas is too dilute to be a significant emitter, but it is possible for it to produce absorption, which has been searched for at X-ray wavelengths but not convincingly detected (Rasmussen et al. 2006).

The radio band provides another approach to detecting hot gas through the hyperfine transitions of ions with magnetic moments, a possibility first discussed by Sunyaev & Churazov (1984) in the context of supernova remnants and galaxy clusters. An advantage to using this approach is that the velocity resolution is far superior relative to current X-ray techniques, permitting one to easily resolve the hyperfine line and obtain a precise line center. The primary disadvantage is that most of the lines are weak, and sometimes at frequencies where it is difficult to make observations.

This transition is a hyperfine spin-flip transition, the same that is responsible for the 21 cm line of neutral hydrogen. It requires that the magnetic moment of an electron interact with the magnetic moment of the nucleus. The magnetic moment is greatest for the electron if there is a single valence electron, so hydrogenic or lithium-like ions are preferred, along with nuclei that have an odd number of protons (or an odd mass number) so that not all the magnetic moments are canceled. The first criteria is easily met, but the second one is more problematic because nature prefers to build atoms with alpha particles, so nearly all of the abundant elements have an even number nuclear charge or an even atomic mass. The two most common elements with odd nuclear charge are hydrogen and nitrogen, the latter being abundant only due to the presence of the CNO cycle in stars. Therefore, it is hydrogenic-like nitrogen (N VII) that has the most favorable hyperfine transition, after the H I 21 cm line (Goddard & Ferland 2003; Sunyaev & Docenko 2006). Unfortunately, the line from $^{14}$N occurs at 53.042 GHz (Shabaev et al. 1995), a frequency regime where there is very significant attenuation due to oxygen resonance lines in the Earth's atmosphere, making low-redshift observations impossible.

Because of this opacity problem, as well as the lack of receivers, most of the attention of observers was focused on the Li-like Fe isotope line, $^{57}$Fe XXIV, which is present in gas near $10^7$ K and has a transition at 98 GHz (D'Cruz et al. 1998), a clear mm window for which there are good receivers. This line was searched for in emission but not detected (Liang et al. 1997), the limits not being very restrictive in regard to model predictions (Goddard & Ferland 2003).

Here we reconsider the emission and absorption possibilities for $^{14}$N, which is two orders of magnitude more common than $^{57}$Fe. Our motivation is that the Green Bank Telescope (GBT) has an excellent receiver in the atmospherically transparent 42–48 GHz range, with a spectrometer that can sample this entire range ($\Delta z = 0.16$) in only four separate settings and with a velocity resolution of 2.7 km s$^{-1}$, which could easily resolve emission or absorption from this ion at its Doppler width (FWHM = 80 km s$^{-1}$ at $10^6$ K). To use this receiver, we are forced to work in the redshift range 0.11–0.26.

This $^{14}$N hyperfine line has atomic properties that make it competitive with the H I hyperfine line for both emission and absorption. It has a critical density of 0.15 cm$^{-3}$, and above this value the emissivity is $\epsilon \propto n_i A_{21}$, where $n_i$ is the density of an element in a particular ionization state and $A_{21}$ is the Einstein $A$-value. For hydrogen, $A_{21} = 2.87 \times 10^{-15}$ s$^{-1}$, while for the N VII line, $A_{21} = 1.99 \times 10^{-10}$ s$^{-1}$ (Sunyaev & Docenko 2006), so even though the nitrogen abundance is $9.1 \times 10^{-5}$ relative to hydrogen (at solar abundance), the difference in the $A$-values compensates so that

TABLE 1
N VII Emission and Absorption Observations

| Number | Name | Type | R.A. | Decl. | $z$ | $t_{exp}$ (min) | $T_a$ (K) | Band | $\nu_{center}$ (GHz) | rms[a] (mK) | Bin Width (km s$^{-1}$) | 1 $\sigma$[b] | Comments |
|---|---|---|---|---|---|---|---|---|---|---|---|---|---|
| 1..... | PKS 0405−12 | Blazar; Sy1.2 | 04 07 48.4 | −12 11 37 | 0.5726 | 32 | 0.31 | 5 | 45.5 | 10.3 | 26.4 | 0.52 | C IV absent at $z = 0.167$ |
| 2..... | PKS 1345+12 | Sy2 | 13 47 33.3 | +12 17 24 | 0.1217 | 32 | 0.47 | 7 | 46.9 | 6.10 | 25.6 | 0.30 | IR bright |
| | | | | | | 32 | 0.41 | 8 | 47.6 | 5.20 | 25.2 | 0.26 | ... |
| 3..... | Abell 1835 | Galaxy cluster | 14 01 02.0 | +02 51 32 | 0.2532 | 24 | ... | 1 | 42.4 | 4.76 | 28.3 | 0.24 | ... |
| | | | | | | 21 | ... | 2 | 43.1 | 4.26 | 27.8 | 0.21 | ... |
| 4..... | Abell 2390 | Galaxy cluster | 21 53 34.6 | +17 40 11 | 0.2280 | 76 | ... | 2 | 43.25 | 2.13 | 27.7 | 0.11 | ... |
| 5..... | 3C 273 | QSO, blazar | 12 29 06.7 | +02 03 09 | 0.1583 | 80 | 16.1 | 5 | 45.4 | 0.34 | 26.4 | 0.017 | Minus 3C 279 |
| | | | | | | 80 | 14.5 | 6 | 46.1 | 0.37 | 26.0 | 0.018 | Minus 3C 279 |
| | | | | | | 32 | 15.8 | 7 | 46.9 | 0.80 | 25.6 | 0.040 | Minus 3C 279 |
| | | | | | | 32 | 12.8 | 8 | 47.6 | 1.00 | 25.2 | 0.050 | Minus 3C 279 |
| 6..... | 3C 279 | QSO, blazar | 12 56 11.1 | −05 47 22 | 0.5362 | 34 | 6.4 | 1 | 42.4 | 0.82 | 28.3 | 0.041 | Minus 3C 345+4C 39.25 |
| | | | | | | 34 | 6.1 | 2 | 43.1 | 1.04 | 27.8 | 0.052 | Minus 3C 345+4C 39.25 |
| | | | | | | 32 | 13.2 | 3 | 43.9 | 0.85 | 27.3 | 0.042 | Minus 3C 345+4C 39.25 |
| | | | | | | 32 | 11.7 | 4 | 44.6 | 1.02 | 26.9 | 0.051 | Minus 3C 345+4C 39.25 |
| | | | | | | 32 | 11.6 | 5 | 45.4 | 0.34 | 26.4 | 0.017 | Minus 3C 273 |
| | | | | | | 32 | 10.5 | 6 | 46.1 | 0.37 | 26.0 | 0.018 | Minus 3C 273 |
| | | | | | | 44 | 3.5 | 7 | 46.9 | 0.80 | 25.6 | 0.040 | Minus 3C 273 |
| | | | | | | 44 | 2.9 | 8 | 47.6 | 1.00 | 25.2 | 0.050 | Minus 3C 273 |
| 7..... | 3C 345 | QSO | 16 42 58.8 | +39 48 37 | 0.5928 | 32 | 3.8 | 1 | 42.4 | 0.89 | 28.3 | 0.044 | Minus 3C 279 |
| | | | | | | 32 | 3.5 | 2 | 43.1 | 1.02 | 27.8 | 0.051 | Minus 3C 279 |
| | | | | | | 30 | 1.9 | 3 | 43.9 | 1.09 | 27.3 | 0.054 | Minus 3C 279 |
| | | | | | | 30 | 1.7 | 4 | 44.6 | 1.29 | 26.9 | 0.064 | Minus 3C 279 |
| | | | | | | 32 | 3.9 | 5 | 45.4 | 0.75 | 26.4 | 0.038 | Minus 3C 279+3C 273 |
| | | | | | | 32 | 3.6 | 6 | 46.1 | 0.64 | 26.0 | 0.032 | Minus 3C 279+3C 273 |
| | | | | | | 24 | 3.6 | 7 | 46.9 | 0.96 | 25.6 | 0.048 | Minus 3C 279+3C 273 |
| | | | | | | 24 | 3.0 | 8 | 47.6 | 1.16 | 25.2 | 0.058 | Minus 3C 279+3C 273 |
| 8..... | 4C 39.25 | QSO | 09 27 03.0 | 39 02 21 | 0.6953 | 32 | 6.4 | 1 | 42.4 | 0.75 | 28.3 | 0.037 | Minus 3C 279 |
| | | | | | | 32 | 5.7 | 2 | 43.1 | 1.05 | 27.8 | 0.052 | Minus 3C 279 |
| | | | | | | 32 | 3.7 | 3 | 43.9 | 0.61 | 27.3 | 0.030 | Minus 3C 279 |
| | | | | | | 32 | 3.2 | 4 | 44.6 | 0.75 | 26.9 | 0.037 | Minus 3C 279 |
| | | | | | | 64 | 2.8 | 5 | 45.4 | 0.41 | 26.4 | 0.020 | Minus 3C 279+3C 273 |
| | | | | | | 60 | 2.6 | 6 | 46.1 | 0.62 | 26.0 | 0.031 | Minus 3C 279+3C 273 |
| | | | | | | 32 | 2.1 | 7 | 46.9 | 1.21 | 25.6 | 0.060 | Minus 3C 279+3C 273 |
| | | | | | | 32 | 1.7 | 8 | 47.6 | 1.38 | 25.2 | 0.069 | Minus 3C 279+3C 273 |

NOTE.—Units of right ascension are hours, minutes, and seconds, and units of declination are degrees, arcminutes, and arcseconds.
[a] Values for Abell 1835, and Abell 2390 are in mK; for the rest, they are in units of $10^{-3}$ of the normalized continuum.
[b] Values for Abell 1835, and Abell 2390 are in K km s$^{-1}$, while uncertainties for other objects are equivalent widths, in km s$^{-1}$.

the volume emissivity is the same for N VII line and the 21 cm line when nitrogen is 1/6 of its solar abundance (comparing equal masses of $10^6$ K gas and H I gas). The N VII emission line will be detectable in this redshift range if $10^{10}$–$10^{11}$ $M_\odot$ of million degree gas is present, which might occur in a cluster of galaxies or an ultraluminous infrared galaxy (ULIRG). The emission line component of our GBT program was to search for such emission from a few different objects.

In absorption, the density of the WHIM is predicted to be between $10^{-4}$ and $10^{-5}$ cm$^{-3}$ (Hellsten et al. 1998), well below the critical density, so all atoms are in their ground state. Thus, unlike the H I 21 cm transition, there is no stimulated emission to reduce the optical depth. The N VII line becomes detectable in absorption for a column density of $10^{20}$–$10^{21}$ cm$^{-2}$ of million degree gas (1/10 solar metallicity), which would occur in a filament 1 Mpc in length and of total particle density $10^{-4}$ cm$^{-3}$. Such column densities can occur, according to simulations (Hellsten et al. 1998), so we have searched for absorption features against strong continuum sources in the 42–48 GHz range.

## 2. DATA PROCESSING

The observations were taken using the 100 m NRAO GBT during the two nights of 2006 February 19 and February 21 in the 42–48 GHz frequency range using the Q-band receiver. The Q-band receiver is divided into two frequency ranges with separate feed and amplifier sets. The GBT spectrometer was configured in its four intermediate frequency (IF) 800 MHz width three-level mode, which allows the observation of two 800 MHz frequency bands in two polarizations at once. Double beam switching was employed such that the source appeared in each of the dual beams alternately for a period of 1 minute. The data were analyzed using GBTIDL (Garwood et al. 2005), version 1.2.1. Bad scans were removed, and the remaining scans were accumulated and averaged. The total useful observing time for each object/band number is listed in Table 1.

Most of the observing time was used to search for absorption lines against strong continuum sources, but the baselines cannot be fit with simple functions, which introduces challenges. Presumably, the structure in the baseline is due to standing waves in the feedhorn and receiver, but this is not well documented yet. To flatten the baseline structure, we tried a variety of procedures, the most successful being a two-step procedure. In the first step, we smooth the spectrum, using adjacent averaging over 200 channels, or about 520 km s$^{-1}$ at 45 GHz (Fig. 1). The original spectrum, in which $T_a$ varies by about 10% of a 0.8 GHz band, is divided by the smoothed spectrum, and this reduces the variation by more than

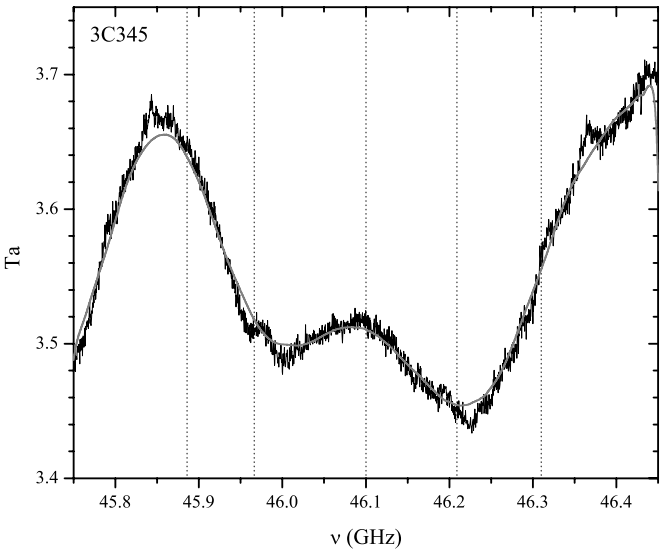


FIG. 1.—Raw antenna temperature (K) from the summed scans for 3C 345 with a 10% variation across the band. The data were smoothed by adjacent averaging 200 bins, a width of about 0.08 GHz (*smooth solid line*). To flatten the spectrum, the first stage is to divide the data by the smoothed data. The dotted vertical lines show the locations of weak lines placed in the spectrum during a test (maximum optical depth is 0.2%). [*See the electronic edition of the Journal for a color version of this figure.*]

an order of magnitude, to less than 1% (Fig. 2). However, most of these variations are systematic in nature and are nearly identical for two different continuum sources observed over similar frequency ranges. These systematics were largely removed by subtracting the fluctuations about unity in one spectrum from the other spectrum, leading to a final rms per bin (an average of 10 channels, or 26 km s$^{-1}$) that was often less than 0.1% of the normalized flux density (Fig. 2).

We tested this procedure by adding spectral lines to a source (3C 345) to see if they were correctly recovered. The tests worked

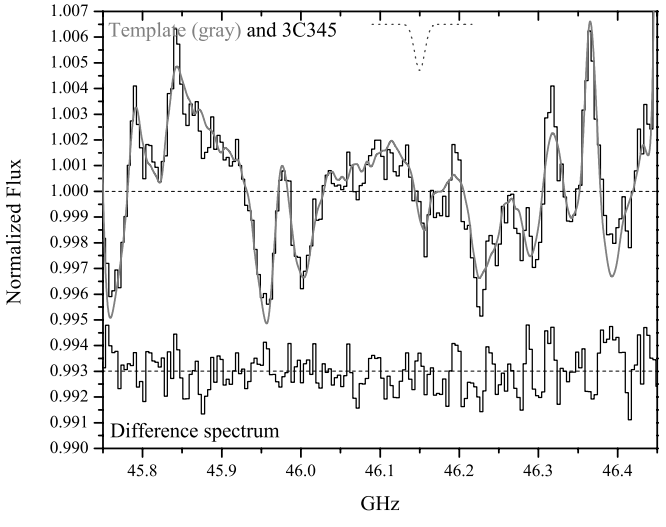


FIG. 2.—Ratio of the data to the smoothed data, in 10 channel bins (26 km s$^{-1}$) for 3C 345 and for the average of 3C 273 and 3C 279. The initial 10% variations are reduced by an order of magnitude. The fluctuations about the unity line are subtracted from the normalized flux of 3C 345 (the difference spectrum), shown at the bottom of the figure and shifted downward by 0.007. This reduces the fluctuations by another factor of 5 in this case, and the resulting rms is similar to the theoretical limit. The type of line that we are searching for is shown as a dotted line in the top of the figure (90 km s$^{-1}$ FWHM, central optical depth of 0.2%). [*See the electronic edition of the Journal for a color version of this figure.*]

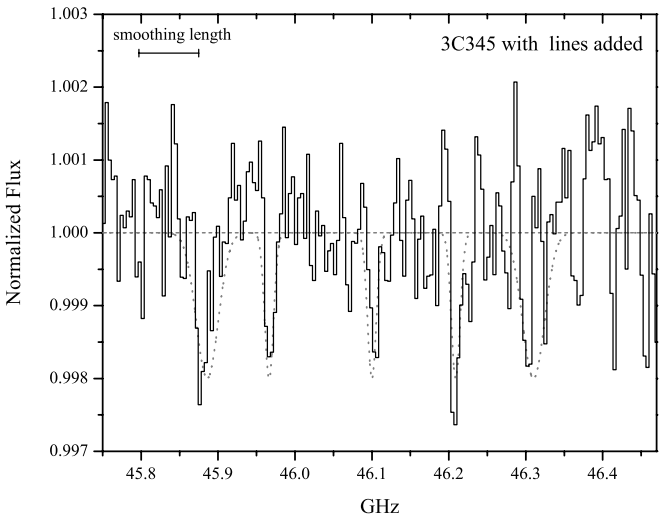


FIG. 3.—Same data set for 3C 345 as above, put processed with five weak lines added to the spectrum of two different widths (*dotted lines*; FWHM of 90 and 200 km s$^{-1}$). The five strongest absorption features are the input lines, which would be recovered by our data reduction procedure. The smoothing length is shown in the upper left. [*See the electronic edition of the Journal for a color version of this figure.*]

well and we successfully recovered absorption lines with central optical depths of 0.002 and widths of 90 and 220 km s$^{-1}$ (FWHM), which are about the line widths anticipated (Fig. 3). Lines as wide as the averaging length will not be recovered reliably, but we should easily be able to detect lines of width 300 km s$^{-1}$ or less.

One aspect of this procedure is that for the final step, one would ideally want to have a strong featureless source, but in general, such a source was either not available or not used. Instead, for a calibration source, we used either 3C 279 or 3C 273, or when both were observed in the same band, the average of the two. When using these sources for the final calibration, a problem can arise if one of the sources has an intrinsic absorption line. This will appear as an emission line in the final spectrum, but this emission line will be present in all final spectra, and as there are either three or four strong continuum sources observed in every band, one can inspect the spectra for this effect, and we have done so. This two-step data processing method was used for 3C 273, 3C 279, 4C

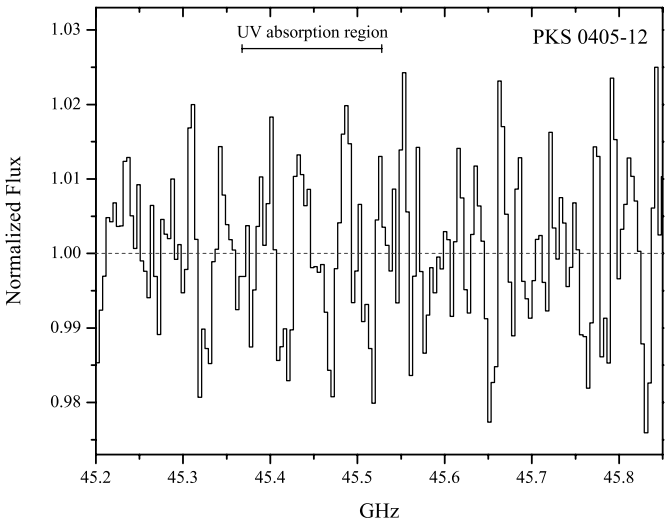


FIG. 4.—Normalized continuum of PKS 0405−12 does not show N VII absorption at the location of the UV absorption lines, which are sensitive to much smaller column densities. The bar is 100 km s$^{-1}$ in length, centered at the UV absorption line redshift.

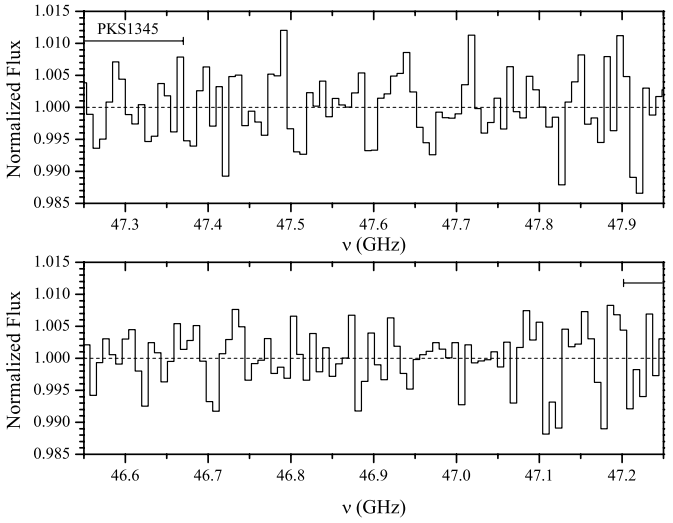


FIG. 5.—Normalized continuum from the IR-bright double-nucleus source PKS 1345+12 shows no emission or absorption from N VII. The horizontal bar is 1000 km s$^{-1}$ in length and is centered on the redshift of the object.

39.25, and 3C 345, and PKS 1345+12, which has a significantly weaker continuum than the others.

For sources with a weaker continuum or without a detectable continuum, we found that subtracting the smoothed continuum from the unsmoothed data worked well. This approach was applied to Abell 1835, Abell 2390, and PKS 0405−12 (at continuum levels of 0.3 K), although for the last source, using the ratio method led to similar results. For Abell 1835, there was a noticeable slow baseline structure after subtracting the smoothed continuum, so we also fit and removed a third-order polynomial fit to the baseline. When observing Abell 2390, PKS 0405−12, and PKS 1345+12, we used overlapping spectral bands to check that if interesting features were observed, the same structures were detected in both observations.

## 3. RESULTS

Most of the observations involved searching for absorption features against the radio continua, but for two clusters of galaxies and one star-forming galaxy, we searched for N VII emission.

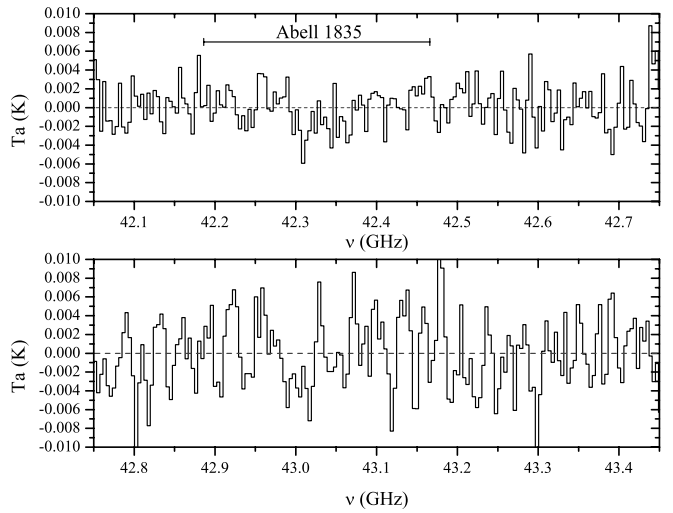


FIG. 6.—Observations from the X-ray bright galaxy cluster Abell 1835 shows no N VII emission. A region 2000 km s$^{-1}$ wide is denoted with a horizontal bar centered at the cluster redshift.

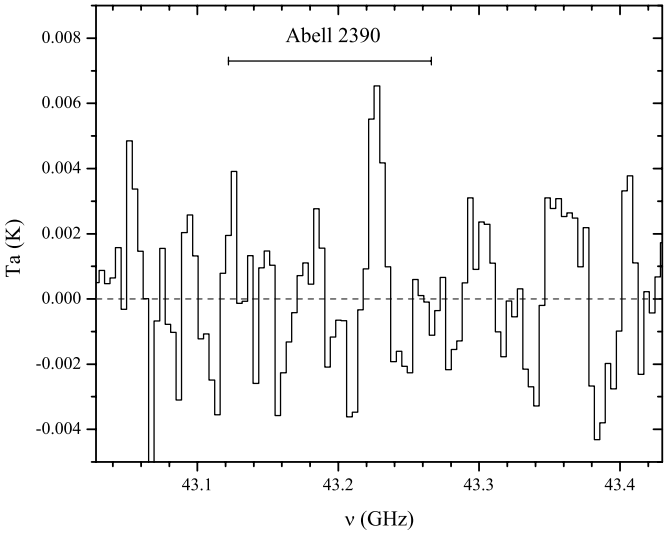


FIG. 7.—Observations of Abell 2390 show a 3.7 $\sigma$ feature that is consistent with the redshift of the cluster, where the horizontal bar is 1000 km s$^{-1}$ in length.

*PKS 0405−12*.—Although the continuum is much lower than most other targets, this was chosen because it has a known C IV and Ly$\alpha$ absorption system at $z = 0.167$ (Spinrad et al. 1993), which would place a N VII absorption line at 45.45 GHz. Two sets of observations were obtained with the central frequency shifted by 0.1 GHz, and the central frequency was different than that of the various strong continuum objects. Possibly for this reason, we were unable to use the second step of our continuum flattening procedure, so the resulting rms is relatively higher than for the strong continuum sources (Fig. 4). There is no evidence for any absorption at the frequency of the N VII transition. The upper limit is not in conflict with the detection of the UV absorption lines, which are sensitive to much lower column densities.

*PKS 1345+12*.—This strong *IRAS* source is similar to Arp 220 in that it has a double nucleus and a great deal of star formation (Xiang et al. 2002). It is also mentioned as a Seyfert 2 galaxy and an IR quasar. We hoped to search for emission due to

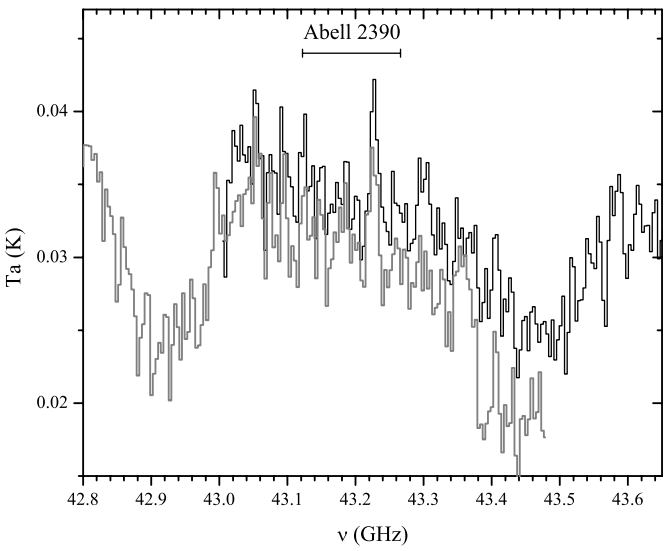


FIG. 8.—Two overlapping spectroscopic observations of Abell 2390, before baseline removal. The strongest emission feature is present in both observations; the horizontal bar is 1000 km s$^{-1}$ wide. [*See the electronic edition of the Journal for a color version of this figure*.]

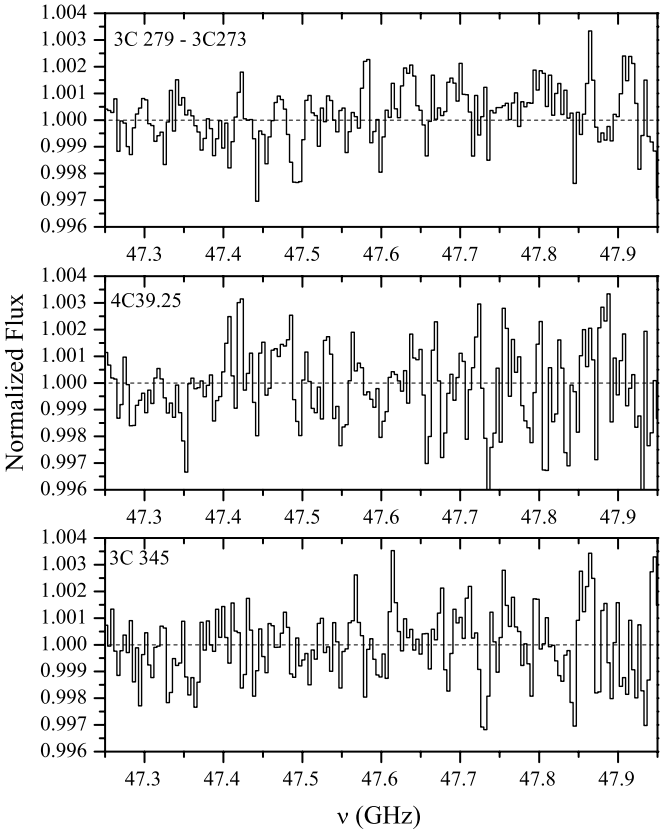


FIG. 9.—Flattened continuum sources in the 47.25–47.95 GHz region (band 8; $0.107 < z < 0.124$ for the N VII line). In the second stage of baseline flattening, 3C 273 and 3C 279 were differenced, while for 4C +39.25 and 3C 345, small baseline residuals were removed by using the average of 3C 273 and 3C 279. The total vertical range is ±0.4%.

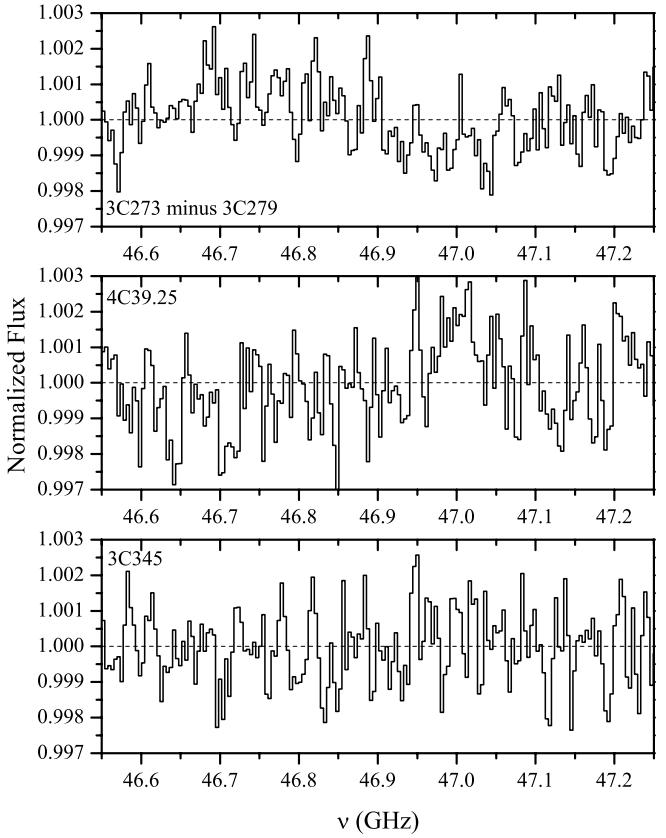


FIG. 10.—Same as above, but for the 46.55–47.25 GHz range (band 7; $0.124 < z < 0.141$). The total vertical range is ±0.3%.

the hot gas from star formation, or for absorption by hot gas against the radio continuum. Two adjacent bands were observed, which included the redshift of the object, but neither emission nor absorption were detected (Fig. 5). An object with a continuum makes it more challenging to detect emission, so the rms is larger than for objects without a significant continuum.

*Abell 1835*.—This cluster of galaxies has strongly centrally concentrated X-ray emission with a cooling time much less than a Hubble time, so it was a classic cooling flow cluster until *XMM-Newton* observations failed to find the expected strong O VII emission (Allen et al. 2001a, 2001b; Peterson et al. 2003). The *XMM-Newton* observations place a limit on the cooling rate of $\sim 50\ M_{\odot}\ \mathrm{yr}^{-1}$. There is no significant radio continuum and there is no detectable emission from the N VII ion (Fig. 6).

*Abell 2390*.—This is another cluster with strong X-ray emission, similar to Abell 1835, but not as luminous and with a lower cooling rate as inferred from pre–*XMM-Newton* data (Allen et al. 2001a, 2001b; Peterson et al. 2003); $H_2$ was detected by Edge et al. (2002). Two observations were obtained where the central frequency was shifted by 0.3 GHz, but both scans included the redshift region of Abell 2390. The common regions were combined and the rms was quite low in the resulting spectrum. No features are detected at or above the 5 $\sigma$ level, which we require for a confident detection. The strongest emission feature is at the 3.7 $\sigma$ level and near the redshift of the galaxy cluster (line flux of $0.51 \pm 0.14$ K km s$^{-1}$, FWHM $= 66 \pm 20$ km s$^{-1}$; Fig. 7). Statistically, a positive feature of this significance occurs 0.01% of the time. The feature is present in both of the individual scans and at about the same strength (Fig. 8). A feature of this strength would have been below the detection threshold in Abell 1835 or PKS 1345+12 due to the higher rms in the spectra. We hope to obtain additional observations to determine the reality of this feature.

*The Strong Continuum Sources*.—The two strong continuum sources 3C 279 and 3C 273 provide the highest S/N continua against which to search for N VII absorption lines. There are no known strong absorption lines in either source over the available redshift range $0.11 < z < 0.26$, although the emission line redshift for 3C 273 lies in the observing range, at 45.8 GHz. We did not observe 3C 273 at frequencies below 45 GHz, so for the 42–45 GHz region, we differenced 3C 279 with 3C 345 and 4C +39.25 to search for absorption features. Since we are differencing spectra, if one should have an absorption line we would see that as an emission line. In the differences of 3C 279 and 3C 273 over the 45–48 GHz band, there were no statistically significant absorption or emission features, with impressively low rms values (5 $\sigma$ upper limits of 0.085–0.25 km s$^{-1}$ for 100 km s$^{-1}$ wide lines; Table 1 and Figs. 9–12). Since no features were seen in this spectral region, we averaged the two spectra and used that average to remove the small variations in the spectra of 3C 345 and 4C +39.45 in the 45–48 GHz range.

In the frequency range 45–48 GHz, there are no significant absorption features in 3C 345 or 4C +39.25 above the 5 $\sigma$ level, so we do not claim detections due to absorption in any of our targets. The strongest feature is found in absorption in the spectrum of 4C +39.25; it occurs in the middle of the 45.0–45.8 GHz band, which has the best response and lowest rms of any band. When we fit for the continuum level, central frequency (45.38 ± 0.04 GHz), line width (FWHM $= 99 \pm 23$ km s$^{-1}$), and equivalent width ($0.19 \pm 0.05$ km s$^{-1}$), the feature has a significance of a 3.8 $\sigma$. Had we fixed some fitting parameters, such as the continuum level, or not

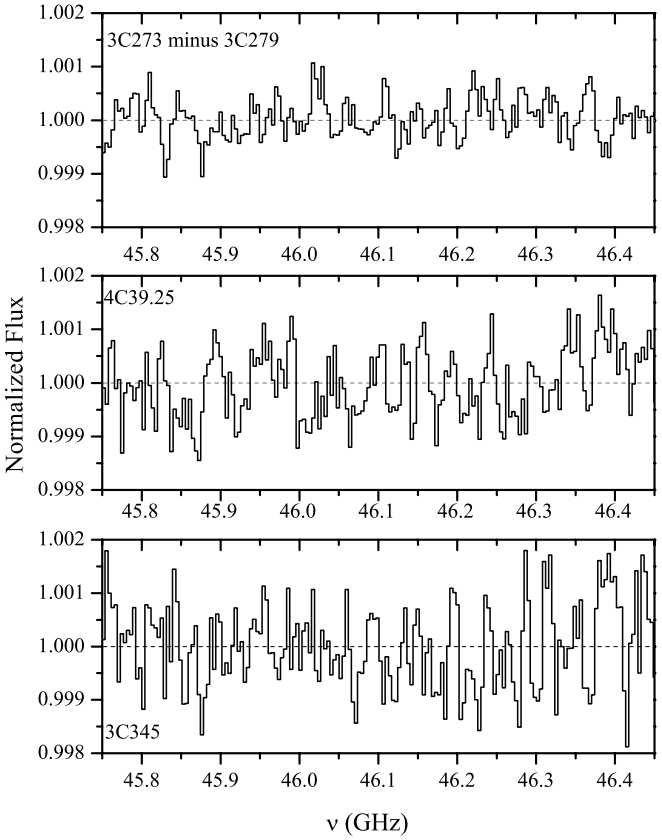


FIG. 11.—Same as above, but for the 45.75–46.45 GHz range (band 6; $0.143 < z < 0.161$). The total vertical range is ±0.2%.

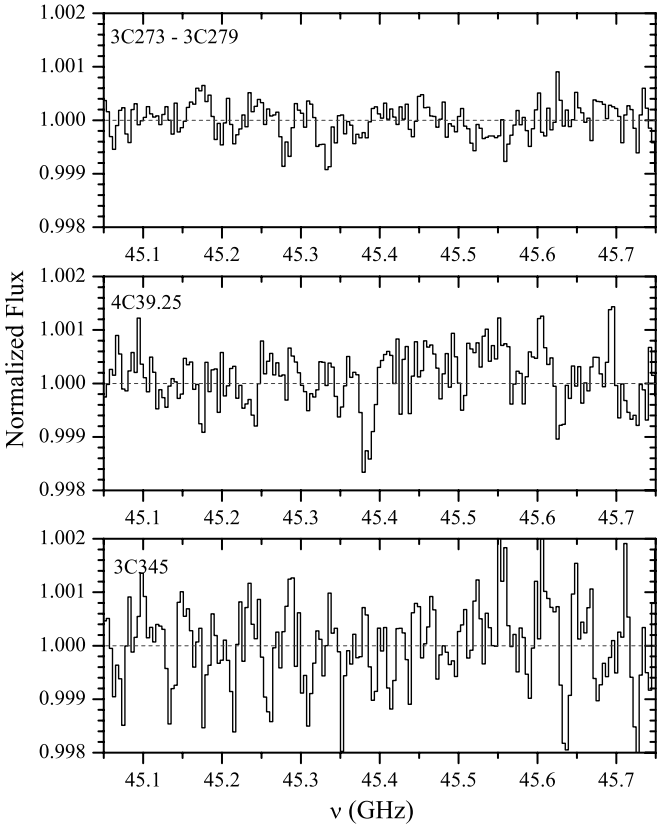


FIG. 12.—Same as above, but for the 45.05–45.75 GHz range (band 5; $0.161 < z < 0.179$). The total vertical range is ±0.2%. The strongest absorption feature in any spectrum occurs in 4C +39.25 at 45.38 GHz, a 3.8 $\sigma$ feature.

fit for certain parameters, such as the line width, the significance would be greater (4.9 $\sigma$). An absorption feature of this strength (3.8 $\sigma$) would occur by chance once in about $10^4$ trials, provided that the noise has a normal distribution. There are about 30–40 independent regions in a single 0.8 GHz band, so for all the bands of all the objects, there were about $10^3$ independent regions in which an absorption feature could have occurred. This feature is rarer than would be expected by chance, but to be cautious, we interpret it as a nondetection until confirmed.

In the frequency range 42–45 GHz, there are no significant features in any object (Figs. 13–16). There are a few features in the 2.5–3 $\sigma$ range, but that is to be expected for the amount of data obtained.

## 4. DISCUSSION AND FINAL COMMENTS

Although we do not detect any emission or absorption features above the 5 $\sigma$ level, we can discuss whether the two strongest features are likely to be confirmed. For this exercise, we compare these features to theoretical predictions.

We can convert the putative line flux seen in Abell 2390 into a luminosity and a mass in the high- and low-density limits. The total observed flux would be $7.3 \times 10^{-19}$ erg cm$^{-2}$ s$^{-1}$, or a luminosity of $9.2 \times 10^{37}$ erg s$^{-1}$ (about 4 orders of magnitude less than the luminosity of the optical and $H_2$ lines). In the limit where the density is greater than the critical density (0.15 cm$^{-3}$), the required gas mass is $1.2 \times 10^{10}$ [N/H] $M_\odot$ and the size would need to be smaller than 11 kpc to achieve this density. This size is encompassed within the beam, which projects to a radius of 36 kpc. The largest mass occurs when the emitting region uniformly fills the beam, and this leads to a density below the critical density and a mass of $6 \times 10^{10}[\mathrm{N/H}]^{-1/2}(T/2 \times 10^6\ \mathrm{K})^{1/4}\ M_\odot$. The mass is confined to a relatively narrow range that is orders of magnitude less than the total gas mass in the system. However, the cooling time for this gas is about $2 \times 10^6$ yr for a gas density of 0.1 cm$^{-3}$, which would lead to an enormous cooling rate in excess of $10^3\ M_\odot$ yr$^{-1}$. For hot X-ray emitting gas to reach the temperature at which N VII occurs, it would have to pass through the temperature range in which O VII is found ($10^6$ K), yet the X-ray upper limits on the O VII emission line strength restrict the cooling rate to $<50\ M_\odot$ yr$^{-1}$ (Peterson et al. 2003). It might be

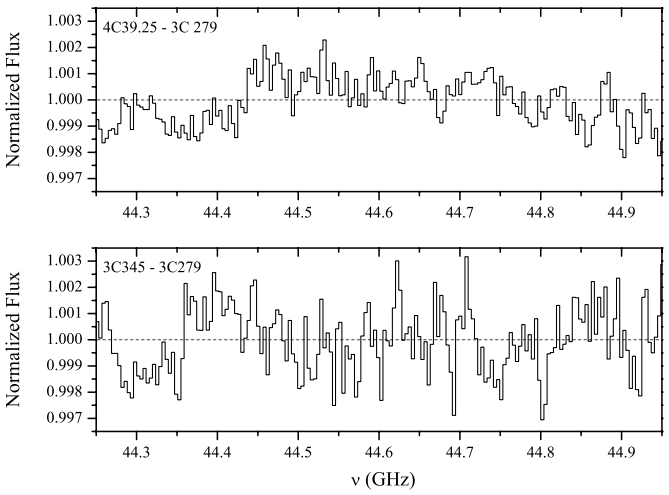


FIG. 13.—Same as above, but for the 44.25–44.95 GHz range (band 4; $0.181 < z < 0.200$). The source 3C 273 was not observed below 45 GHz, so the continuum of the strong source 3C 279 was used to remove small baseline residuals from 4C +39.25 and 3C 345. The total vertical range is ±0.35%.

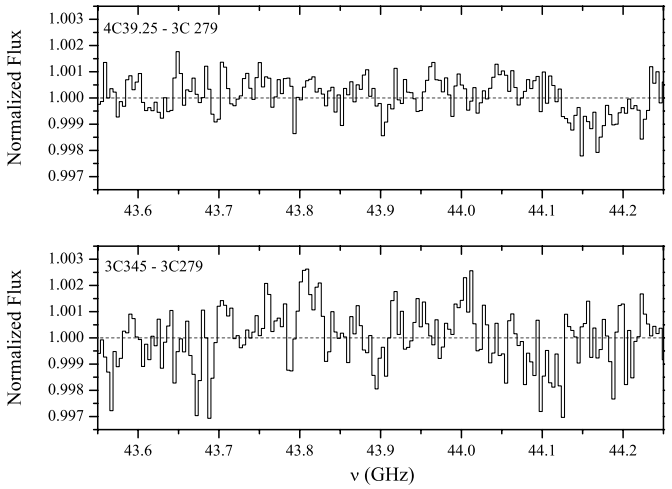


FIG. 14.—Same as above, but for the 43.55–44.25 GHz range (band 3; $0.200 < z < 0.219$).

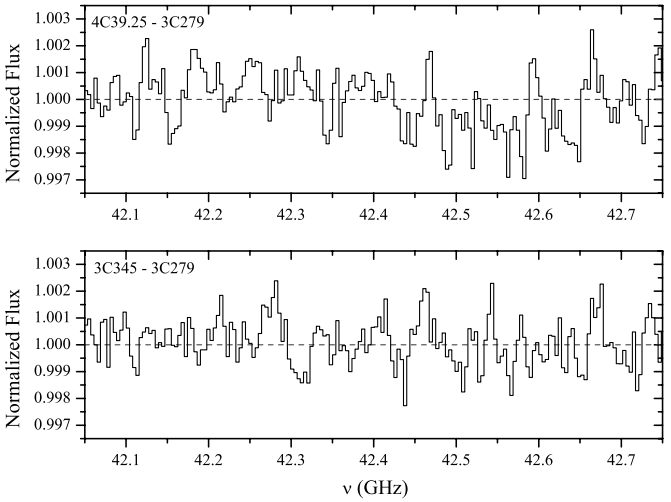


FIG. 16.—Same as above, but for the 42.05–42.75 GHz range (band 1; $0.242 < z < 0.263$).

possible to find a model in which the O VII is suppressed while the N VII is visible, but until such a model is found the current theoretical expectations would suggest that this emission feature in Abell 2390 is unlikely to be real.

The other feature of note is the absorption feature in 4C +39.25, which can be converted into a column density for comparison with expectations. In the optically thin limit, we can use the usual linear relationship between the fractional equivalent width and the column density to obtain $N(\mathrm{N\ VII}) = 1.6 \times 10^{16}\ \mathrm{cm}^{-2}$. However, this value does not take into account the excitation rate corrections due to the interaction with the cosmic microwave background, as discussed by Sunyaev & Docenko (2006). At $z = 0.17$, this reduces the cross section by a factor of 0.29. Including this, the implied total column density is, for an ionization fraction of 0.5, $N = 1.3 \times 10^{21}(Z/Z_{\odot})^{-1}\ \mathrm{cm}^{-2}$. If this were to represent a modest overdensity filament, and the filament is typically 2 Mpc in diameter (Springel et al. 2005; or greater, if we are looking along a filament), the gas density would be $2 \times 10^{-4}\ \mathrm{cm}^{-3}$. While this seems feasible, it is larger than the columns that Hellsten et al. (1998) predict. We have used the temperatures, densities, and metallicities from their simulations to determine the highest column densities in their simulations, covering a redshift range of $\Delta z = 0.3$, which is comparable to the total path length sampled by all strong continuum sources ($\Delta z = 0.43$). Their simulation implies a maximum column of $N(\mathrm{N\ VII}) = 1 \times 10^{15}\ \mathrm{cm}^{-2}$, about 50 times lower than the column associated with this feature. Their metallicity is 0.08 $Z_{\odot}$ at the location of this absorption feature, and it is hard to imagine that it could be more than a factor of a few higher, which would not make their predicted column detectable. A similar conclusion is reached by Sunyaev & Docenko (2006), who also considered the recent models of Cen & Fang (2006). Since the model prediction is more than an order of magnitude lower than the N VII column density associated with this feature, it is unlikely to be a real absorption feature.

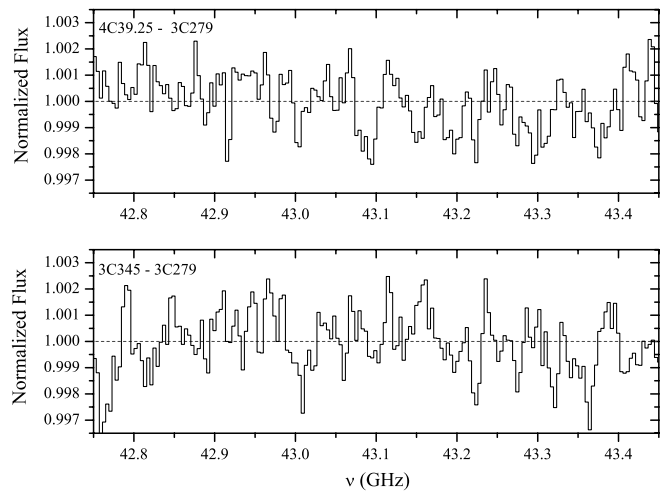


FIG. 15.—Same as above, but for the 42.75–43.45 GHz range (band 2; $0.222 < z < 0.242$). The feature in the 4C +39.25 spectrum near 43.1 GHz is a 2.7 $\sigma$ feature and such features are expected for the amount of data obtained and the number of independent spectral resolution elements.

In the 40–50 GH range, the sources chosen for absorption studies are the brightest sources available, but for emission line studies, the best targets are at a redshift too low to be accessible with the current receiver. For example, the two best galaxy clusters would be Abell 2597 and Abell 426 (the Perseus cluster), as both show strong evidence for cooling gas, at rates of 30–50 $M_{\odot}\ \mathrm{yr}^{-1}$ (Morris & Fabian 2005; Bregman et al. 2006). However, their redshifts place the N VII line at 49.0 and 52.2 GHz. Observations at 52.2 GHz may never be feasible due to atmospheric extinction, but observations at 49.0 GHz may be possible with modifications to the GBT receiver. Similarly, there are nearer galaxies with very active star formation (i.e., 10035+4852, 10565+2488) and nearer X-ray bright elliptical galaxies (i.e., NGC 6414 and KIG 412), but this would demand that observations be made in the 50–51 GHz range, which is currently not possible. At these frequencies, the opacity decreases with altitude, so observing at the ALMA site has several advantages, although in the current plan a 50 GHz receiver will not be available.

For purposes of detecting absorption by dilute gas in the million degree range, it is valuable to compare the columns detectable using the hyperfine N VII line and the X-ray lines of O VII and O VIII. At X-ray energies, O VII absorption is the best line to detect and toward the brightest sources it has been detected (at $z = 0$) for $N(\mathrm{O\ VII})$ of $10^{16}\ \mathrm{cm}^{-2}$. These exposures typically require 300 ks to reach this detection threshold. Our N VII observations are sensitive to a column density about 6 times larger, but since nitrogen is 6 times less common than oxygen, the equivalent total gas column needs to be correspondingly greater (about a factor of 30). However, our limits were obtained in less than an hour of integration time, 2 orders of magnitude shorter than the X-ray observations.

For the radio observations, if the rms decreases with the square root of the integration time, a 30 hr observation would yield a sensitivity for N VII that is within a factor of 5 of the sensitivity of O VII measurements in the X-rays.

One future goal is to determine whether the rms of a radio continuum continues to decrease with longer integration times. The current observations have an rms that is near the theoretical value, but to achieve it we used a two-step procedure to flatten the continuum and remove the standing wave structure. It would be immensely helpful if the amplitude of the standing waves could be reduced at the feedhorn and receiver region. The most immediate goal is to either confirm or refute the two strongest features, and this can be accomplished by longer integrations and by using a variety of different settings when observing the same object (e.g., different central frequency, changing the focus by fractional wave amounts).

We would like to thank the GBT staff for their considerable help, and in particular to Frank Ghigo, Ron Madellena, and Jay Lockman. J. N. B. would like to thank Mort Roberts, Dave Hogg, and Robert Brown for their encouragement in pursuing this project. Partial financial support was provided by the NRAO, which is operated under contract for the NSF by Associated Universities, Incorporated.

REFERENCES

Allen, S. W., Ettori, S., & Fabian, A. C. 2001a, MNRAS, 324, 877
Allen, S. W., Schmidt, R. W., & Fabian, A. C. 2001b, MNRAS, 328, L37
Bregman, J. N., Fabian, A. C., Miller, E. D., & Irwin, J. A. 2006, ApJ, 642, 746
Cen, R., & Fang, T. 2006, ApJ, 650, 573
D'Cruz, N. L., Sarazin, C. L., & Dubau, J. 1998, ApJ, 501, 414
Edge, A. C., Wilman, R. J., Johnstone, R. M., Crawford, C. S., Fabian, A. C., & Allen, S. W. 2002, MNRAS, 337, 49
Garwood, R., Braatz, J., Marganian, P., & Radziwill, N. 2005, BAAS, 37, 1212
Goddard, W. E., & Ferland, G. J. 2003, PASP, 115, 647
Hellsten, U., Gnedin, N. Y., & Miralda-Escudé, J. 1998, ApJ, 509, 56
Liang, H., Dickey, J. M., Moorey, G., & Ekers, R. D. 1997, A&A, 326, 108
Morris, R. G., & Fabian, A. C. 2005, MNRAS, 358, 585
Peterson, J. R., Kahn, S. M., Paerels, F. B. S., Kaastra, J. S., Tamura, T., Bleeker, J. A. M., Ferrigno, C., & Jernigan, J. G. 2003, ApJ, 590, 207
Rasmussen, A. P., Kahn, S. M., Paerels, F., Willem den Herder, J., Kaastra, J., & de Vries, C. 2007, ApJ, 656, 129
Shabaev, V. M., Shabaev, M. B., & Tupitsyn, I. I. 1995, Phys. Rev. A, 52, 3686
Spinrad, H., et al. 1993, AJ, 106, 1
Springel, V., et al. 2005, Nature, 435, 629
Sunyaev, R. A., & Churazov, E. M. 1984, Soviet Astron. Lett., 10, 201
Sunyaev, R. A., & Docenko, D. 2006, Astron. Lett., 33, 67
Xiang, L., Stanghellini, C., Dallacasa, D., & Haiyan, Z. 2002, A&A, 385, 768